

Original Article

# Numerical and Experimental Analysis on Airfoil for Micro-Scale Horizontal Axis Wind Turbine

Sanket S. Unde<sup>1\*</sup>, D. B. Jadhav<sup>1</sup>, Akshay A. Harale<sup>1</sup>, Yuvraj V. Thorat<sup>1</sup>

<sup>1</sup>Department of Mechanical Engineering, Bharati Vidyapeeth (Deemed to be University), College of Engineering, Pune, Maharashtra, India.

\*Corresponding Author : [ssunde@bvucoep.edu.in](mailto:ssunde@bvucoep.edu.in)

Received: 20 May 2023

Revised: 29 July 2023

Accepted: 05 August 2023

Published: 15 August 2023

**Abstract** - Objective: Most researchers worldwide have studied large and medium-scale wind turbines. Small and micro-scale wind turbine research has been explored for various applications. The present study emphasizes the development of a blade profile for micro-scale wind turbines. Methods: A new airfoil was designed for horizontal axis microscale wind turbines using Q-Blade simulation software. An airfoil three-dimensional model was developed in solid works. Ansys Fluent was used to perform CFD simulations of two and three-dimensional models of airfoils having an angle of attack (AoA) ' $\alpha$ ' in the  $0^0$  to  $15^0$  range. Findings: Simulation results obtained through CFD and Q-Blade were compared with wind tunnel experimental results. Q-Blade, CFD simulation, and experimental wind tunnel results reveal that with the increase in AoA up to  $5^0$ , the lift-to-drag coefficient ( $C_l/C_d$ ) increases, and after that, it drops down. Novelty: Q-Blade and CFD simulation have the potential to minimize the dependency of the researchers on experimentation.

**Keywords** - Lift coefficient ( $C_l$ ), Drag coefficient ( $C_d$ ), Wind turbine, Airfoil, Micro-scale, Horizontal axis, Angle of attack (AoA) ' $\alpha$ '.

## 1. Introduction

Renewable power capacity of India till 31<sup>st</sup> March 2022 was 109885.38 MW. Solar power, wind power and biomass power contribution were 53996.54 MW (49.1%), 40357.58 MW (36.7%) and 10205.61 MW (9.3%) respectively [1]. The wind turbines are categorized according to their capacities of power generation viz; micro (50 W- 2 kW), small (2.1 kW- 40 kW), medium (40.1 kW- 999 kW) and large (1 MW - 6MW) [2]. Large-capacity wind turbine farms may lead to significant weather changes [3,4]; hence to avoid this, the use of micro to small-capacity wind turbines was preferred for domestic applications. Their keen observation was work is necessary to be done on the study of the effect of airfoils on the performance of wind turbines [5]. Bukala et al. [6] reported that the Weibull or Rayleigh probability distributions model gives better estimates of wind energy generation than those obtained using the yearly wind speed of the location. Abdoukader Ibrahim Idriss et al. [7] applied the Weibull probability distribution model with two parameters for wind prediction. It provides better results while analyzing variable data. Lee et al. [32] applied baseline blade theory (BBT) and blade element momentum theory (BEMT) for the design of a blade. The power coefficient obtained using BEMT was 50% more than that of BBT. Kazumasa Ameku et al. [9] designed the thin airfoil blade for 3 KW power. It was capable of generating an output of 1105 W, having a coefficient of power

of 0.14[8]. Pourrajabin A. et al. [10] designed the micro-scale wind turbine blade of the horizontal axis for low wind speed using a genetic algorithm optimization technique. The chord and twist of an airfoil were optimized for 0.5, 0.75 and 1 kW capacity. Ozgener [11] performed an optimization analysis of a small-scale wind turbine blade. They recommended that the blade profile should be optimized within the constraint of its aerodynamic property. Ankan Dash [12] analyzed the NACA 0012 at various angles of attack with a constant Reynolds number for wind turbine airfoils. He reveals that CFD analysis is a proficient substitute for the experimental method. Jin Yao et al. [13] analyzed the airfoil aerodynamic work and results compared with the experimental data. Rodrigues et al. [14] suggested guidelines for developing small-capacity wind turbines using scrap material. Abdulkadir ali et al. [33] analyzed the various tip configuration for the wind turbine of the horizontal axis.

Monteiro et al. [16] performed the testing of a wind tunnel for the wind turbine rotor of the horizontal axis. Experimental and simulation results with two blade element momentum codes match closely[15]. It was concluded that the proper selection of small-scale wind turbines for airfoil and optimized rotor blades are necessary [17]. Choubey et al. [18] performed the CFD analysis and concluded that the optimal power is



obtained at an angle of  $10^\circ$  out of the remaining angles of attack  $0^\circ$ ,  $10^\circ$ ,  $15^\circ$  and  $30^\circ$  with a wind velocity of 4 m/s. Ani [19] found that hybrid PV/wind system shows better results in terms of Net Present Cost (NPC). The wind turbine with three rotor blades achieves maximum efficiency at the tip speed ratio in the range of 6-8 [20]. N. Bizzarrini et al. [21] investigated the methods to minimize energy costs with the key elements. The energy capture to energy loading ratio of tailored airfoils was found to be enhanced due to its aerodynamic nature. A wind turbine blade is categorized as tip, mid and root.

The root part plays an important role during structural considerations, while the tip part is during aerodynamic considerations. Ernesto Benini et al. [22] studied the designs of HAWT to maximize its annual energy production (AEP) and minimize the cost of energy (COE) produced. COE and AEP were found to be mostly influenced by turbine size and rated power. Xiongwei Liu et al. [23] Optimized the slope between the blade chord and twisted angle with a linear, radial profile for a fixed-pitch, fixed, speed turbine. It enhances power performance with minimum manufacturing cost.

Small and micro-scale wind turbine efficiency relies on; airfoil profile selection, number of blades and environmental conditions. Airfoil aerodynamic properties influence the efficiency of wind turbines. The present work emphasizes airfoil profile design and analysis for a microscale wind turbine of a horizontal axis using Q-Blade and ANSYS fluent software. The Q-Blade and Ansys fluent CFD results are moderately matched for the predicted  $C_l/C_d$  ratio at  $\alpha = 5^\circ$ .

## 2. Design and Simulation of an Airfoil using Q-Blade

Wind turbine aerodynamic simulation can be performed using open-source Q-Blade software. The airfoil analysis and design tool (XFOIL) is incorporated into Q-Blade software. The integration in XFOIL allows users to compute the performance curve of the airfoil [34]. The maximum camber of the designed airfoil was 4.75% of the chord; it is situated at 46.20% of the chord from the leading edge and has a maximum thickness of 12.93% of the chord at 30%. The airfoil was designed for high lift with minimum drag coefficients.

The airfoil was investigated for thrust, power, drag and lift coefficient. The simulation was performed by keeping wind speed, kinematic viscosity, Reynolds number and air density constant. The values of these parameters were 12 m/s,  $1.79 \times 10^{-5}$  kg-m/s, 823000,  $1.23 \text{ kg/m}^3$  and respectively. The AoA varied from  $0^\circ$  to  $15^\circ$ . Fig. 1 represents the designed airfoil profile using Q-Blade software.

### 2.1. Q-Blade Simulation Results

From fig. 2, it is observed that there is a linear increase in  $C_l/C_d$  ratio till  $\alpha$  reaches 50, and after that, it decreases gradually. At  $\alpha = 50$ ,  $C_l$ ,  $C_d$ , and  $C_l/C_d$  ratios were 1.028, 0.0085 and 120.94, respectively.

The assumption of a horizontal axis wind turbine is based on maximum lift force, and a low Reynolds number airfoil allows it to rotate at low speed with a low  $\alpha$  angle [24, 25].

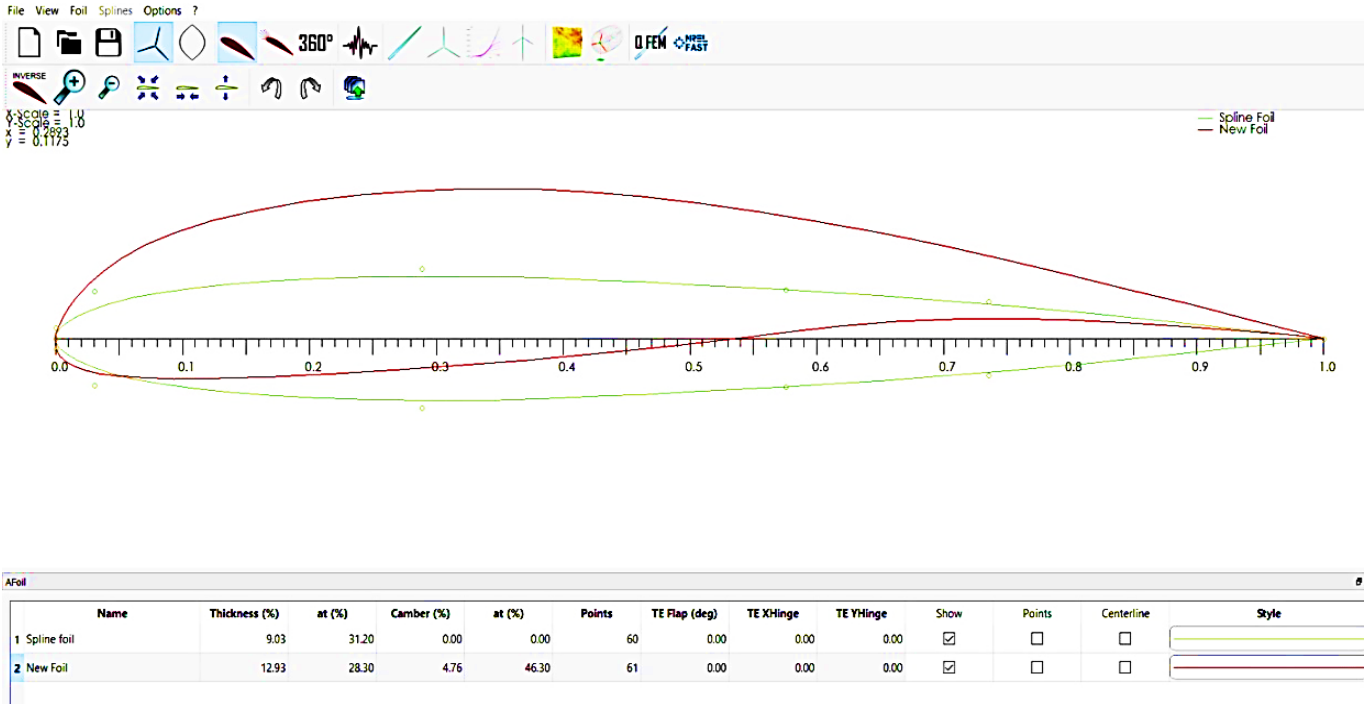


Fig. 1 A newly designed airfoil

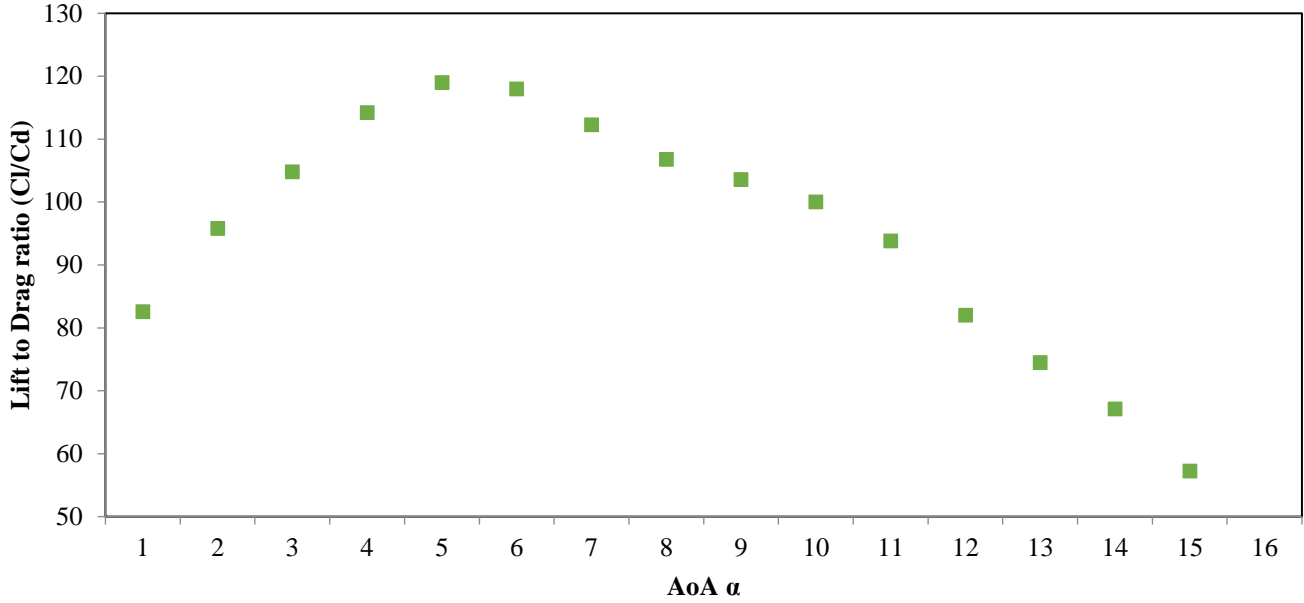


Fig. 2  $C_l/C_d$  ratio vs  $\alpha$

The airfoil profile was changed from the rotor to the tip section, and its aerodynamic properties were examined at different blade sections. Optimum rotor theory was used to estimate the shape of the blade having a midpoint radius 'r' [16].

Fig. 3 represents the rotor blade assembly developed using Q-Blade software. The blade was discretized into ten equal elements, each having a length of 0.08 m. Chord length at the start and end positions were 0.117 m and 0.031 m, respectively.

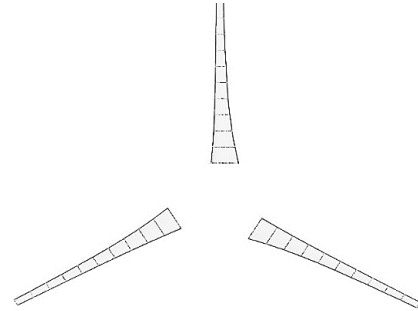


Fig. 3 Designed rotor blade model

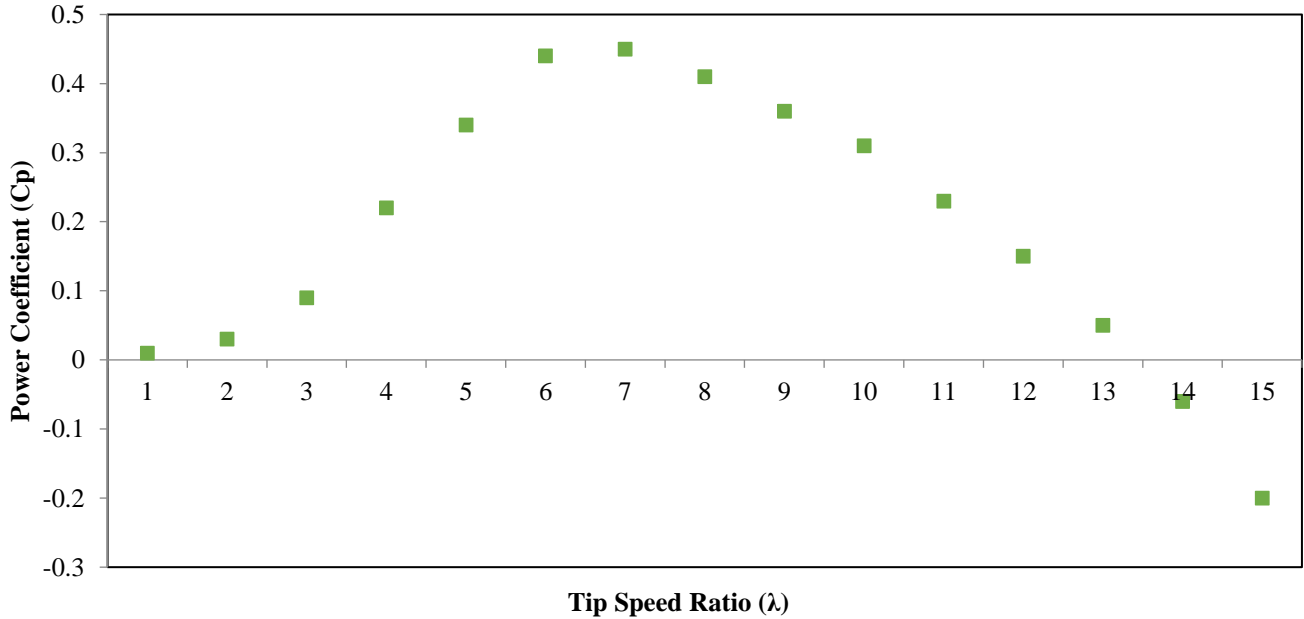


Fig. 4 Power coefficient ( $C_p$ ) vs tip speed ratio ( $\lambda$ )

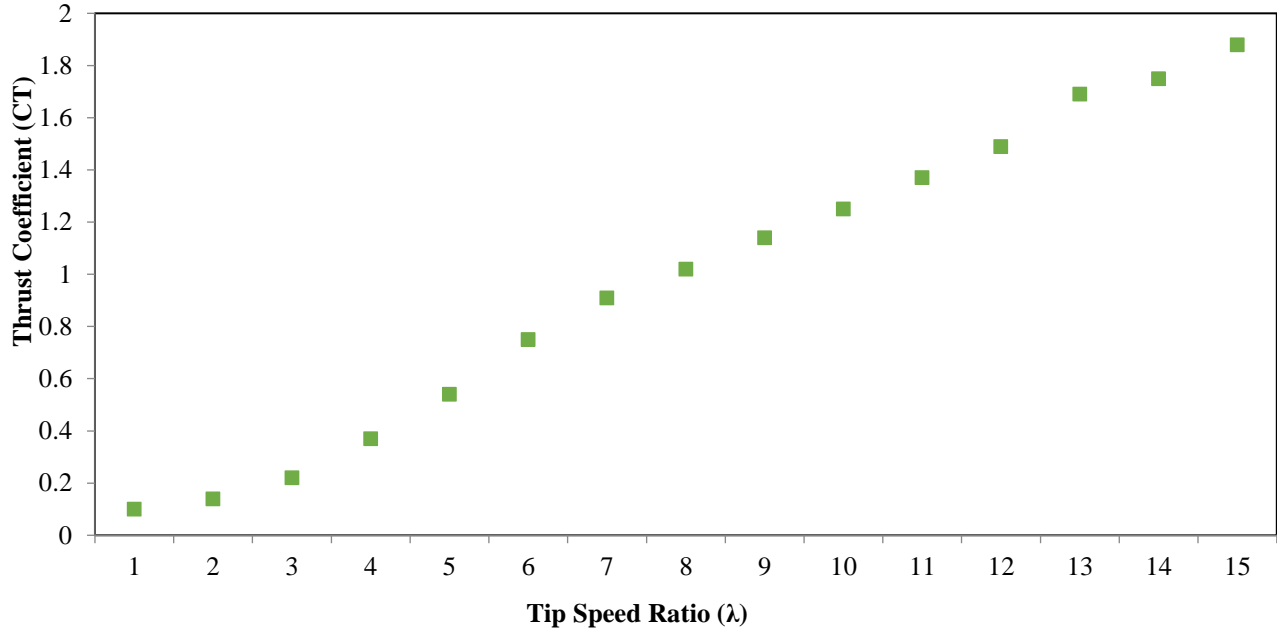


Fig. 5 Thrust coefficient (CT) vs tip speed ratio (λ)

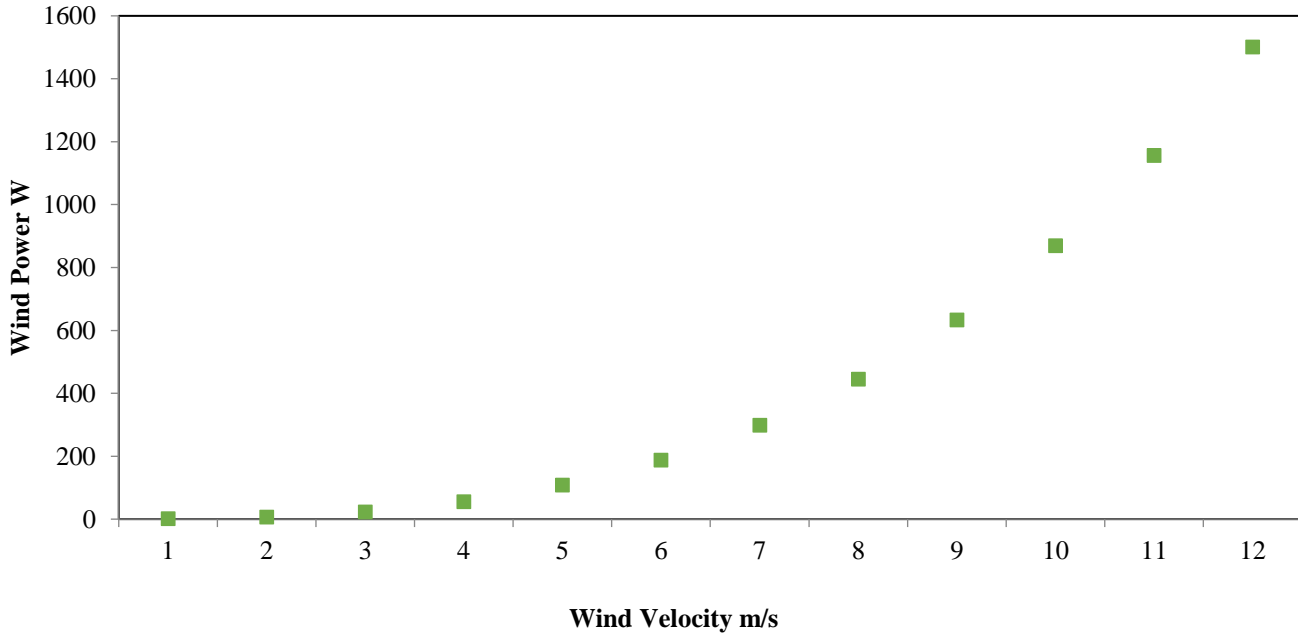


Fig. 6 Wind power vs Wind velocity

During the simulation, wind speed and tip speed ratio ( $\lambda$ ) ranged between 0-12 m/s and 1-15. Fig. 4 depicts that at a zero tip speed, the rotor will not rotate and therefore has zero power coefficient. The power coefficient is high at a tip speed ratio of 7.

Therefore, a tip speed ratio of 7 was selected for blade design with a power coefficient of 0.45. Ronit K. Singh and M. Rafiuddin [26] designed and tested a new airfoil for 3-6 m/s wind speed. For 6 m/s wind speed, they obtained a maximum power coefficient of 0.29.

Fig. 5 depicts that  $\lambda$  is directly proportional to the thrust coefficient (CT). The maximum value of the thrust coefficient is unity for axial induction factor 0.5 and is less than or equal to 0.96 for axial induction factor 0.33 [16]. From the simulation, it was observed that at  $\lambda = 7$ , the CT = 0.91.

From fig. 6, the blade cannot rotate until wind velocity reaches 3 m/s due to insufficient thrust. Wind power and velocity have a linear relationship during the wind velocity range of 3-8 m/s, which was exponential during 8-12 m/s.

### 3. 2D CFD Simulation of an Airfoil

Energy, momentum and continuity equations are the backbone of CFD. Finite volume and difference methods are used to discretize the partial differential equations. The present work examined turbulent flow using Reynolds averaged Navier-Stokes (RANS). 3.1. 2D CFD Simulation of Airfoil

Fig. 7 represents the airfoil surface obtained through a profile that passes through the vertices. Fig. 8 shows C- Mesh and rectangle domains with ten and twenty-time chord lengths, respectively, were created from the tail of the airfoil. The airfoil was subtracted from the domain. A good quality mesh was obtained using forward and reverse bias factors 150. The number of element divisions for the edge towards the airfoil and round edge was selected as 50 and 100, respectively. Fig. 9 represents the mesh near the airfoil; 4500 element consists in this meshing out of 500 elements on the airfoil. Fig.10 shows the domain labeled as airfoil, inlet and outlet.

The standard wall function of turbulent model k- $\epsilon$  was selected. A bluff body surrounded by air having a low Reynolds number can be precisely simulated using this model. It gives good results for large pressure gradients at boundary layers. Kevadiya et al. [28] examined a 2D analysis of NACA 4412 airfoil at an angle of  $0^\circ$  to  $12^\circ$  and a constant Reynolds number of 100000. The density, kinematic viscosity of air was taken as  $1.23 \text{ kg/m}^3$  and  $1.785 \times 10^{-5} \text{ kg/m-s}$ , respectively. The wind speed is kept constant at 12 m/s. The wall was considered stationary and should follow the condition of no sleep shear. The semi-implicit CFD algorithm was preferred for performing the simulation [27].

#### 3.1. 2D CFD Simulation Result and Discussion

Fig. 11 states that at  $\alpha = 5^\circ$ , the  $C_l/C_d$  ratio reaches its maximum value of 49.04, and after that, it decreases due to an increase in drag force. The corresponding  $C_l$  and  $C_d$  coefficients were 1.09 and 0.023. Douvi et al. [25] concluded that the high AoA does not provide correct results for the turbulent model in commercial CFD software.

Fig. 12 (a-f) represents the pressure distribution contours corresponding to  $\alpha$  values lying between  $0^\circ$  to  $15^\circ$ . The simulation was performed on a structured grid using a pressure-based solver. Airfoil top surface and leading edge were subjected to low and high pressure, respectively. As the value of  $\alpha$  increases, subsequently, the pressure on the lower side of airfoil walls increases. The lift force will force the airfoil in an upward direction. For  $\alpha$  angle,  $3^\circ$  to  $5^\circ$  pressures at the lower surface of the airfoil is a more, and the upper surface drag is less, which results in a maximum  $C_l/C_d$  ratio.

The flow velocity was observed to be approximately zero at the leading edge (stagnation point); hence the separation of the boundary layer started occurring, as represented in fig. 13 (a-f). The velocity of the stream was found to be the utmost for an airfoil top surface, while at the bottommost surface, it is found to be reduced. As the AoA reaches  $10^\circ$  or above, the backflow is generated (vortex) at the trailing edge. The generated back flow increases the drag, which leads to a reduction in the efficiency of the blade.

Hence it is essential to keep AoA at maximum  $C_l$  to minimum  $C_d$ . At the trailing edge, boundary layer separation increases with increasing  $\alpha$  angle. After angle  $15^\circ$ , strain drag is high at the trailing edge.

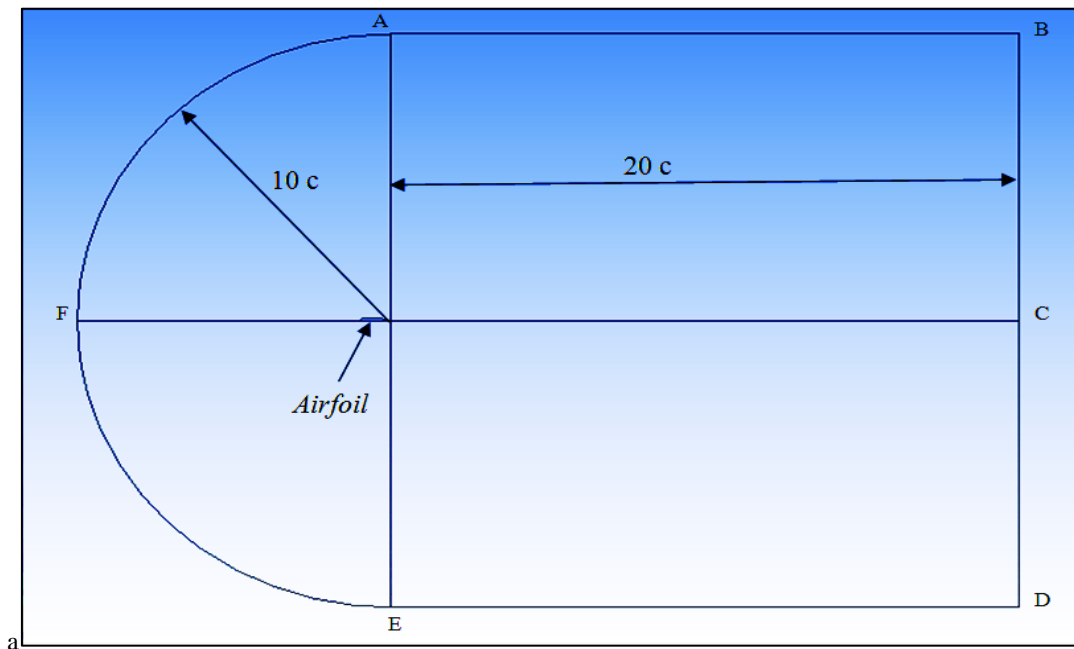


Fig. 7 Computational domain of airfoil

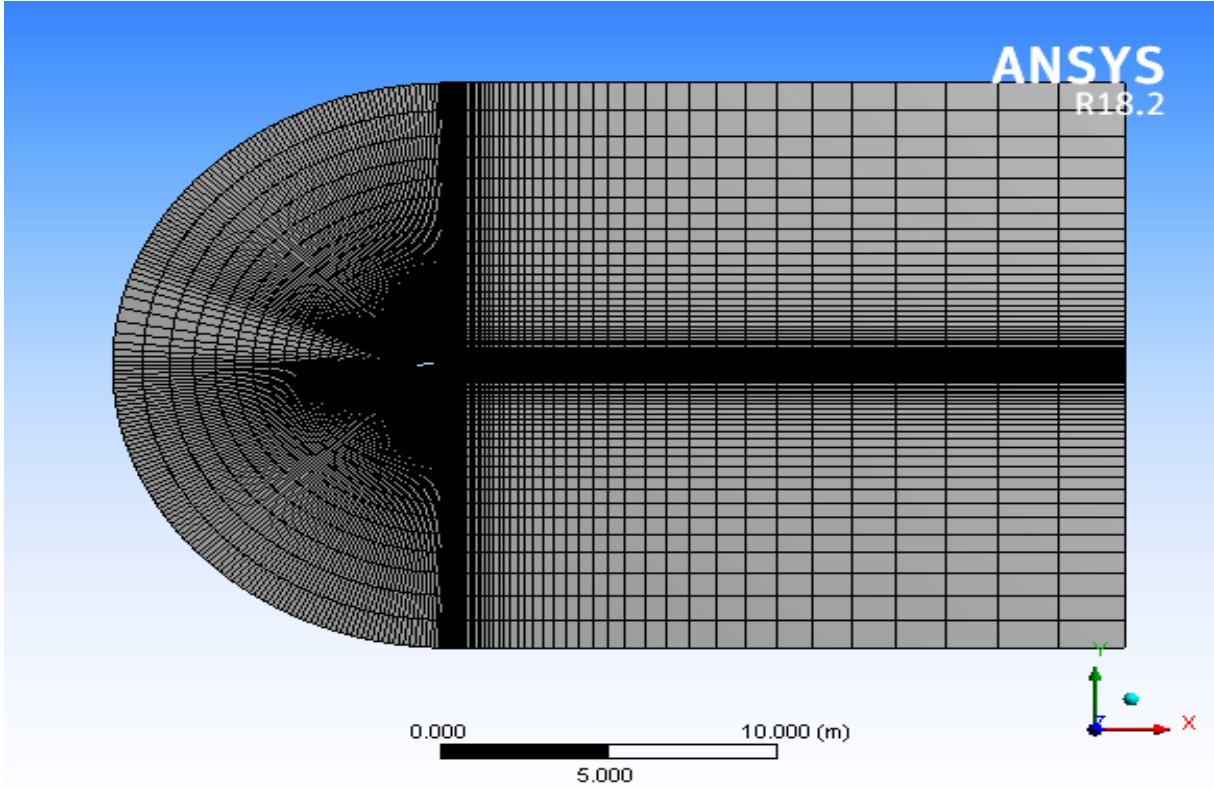


Fig. 8 Meshing domain of airfoil

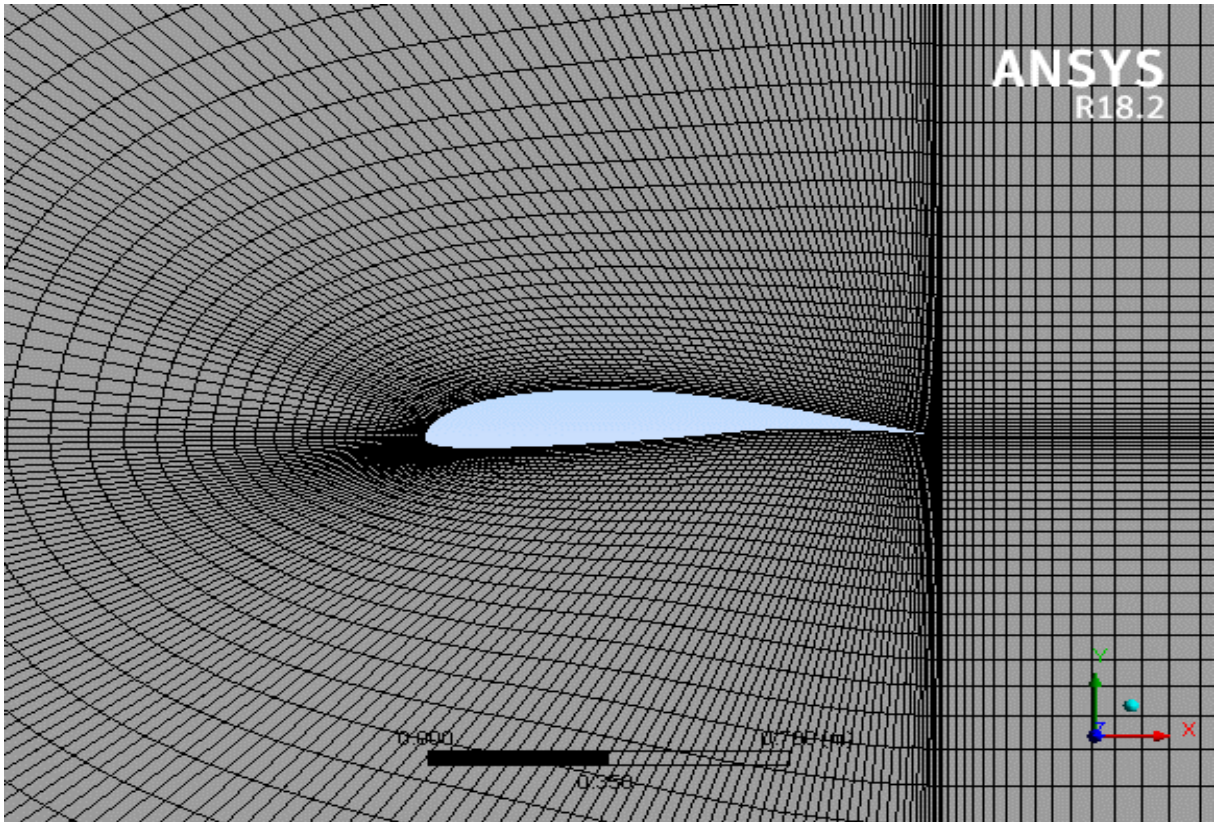


Fig. 9 Meshing around the airfoil

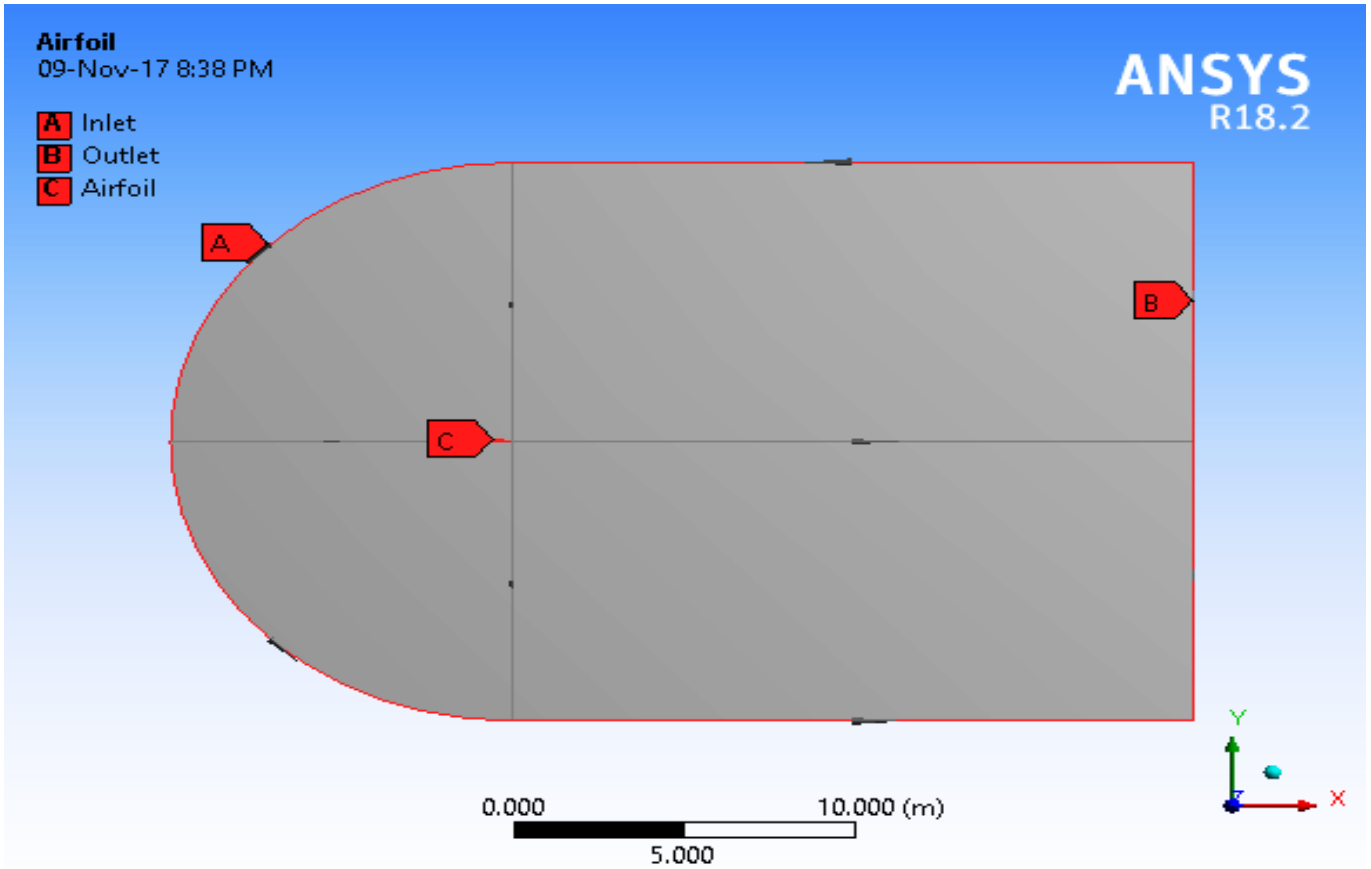


Fig. 10 Name selection

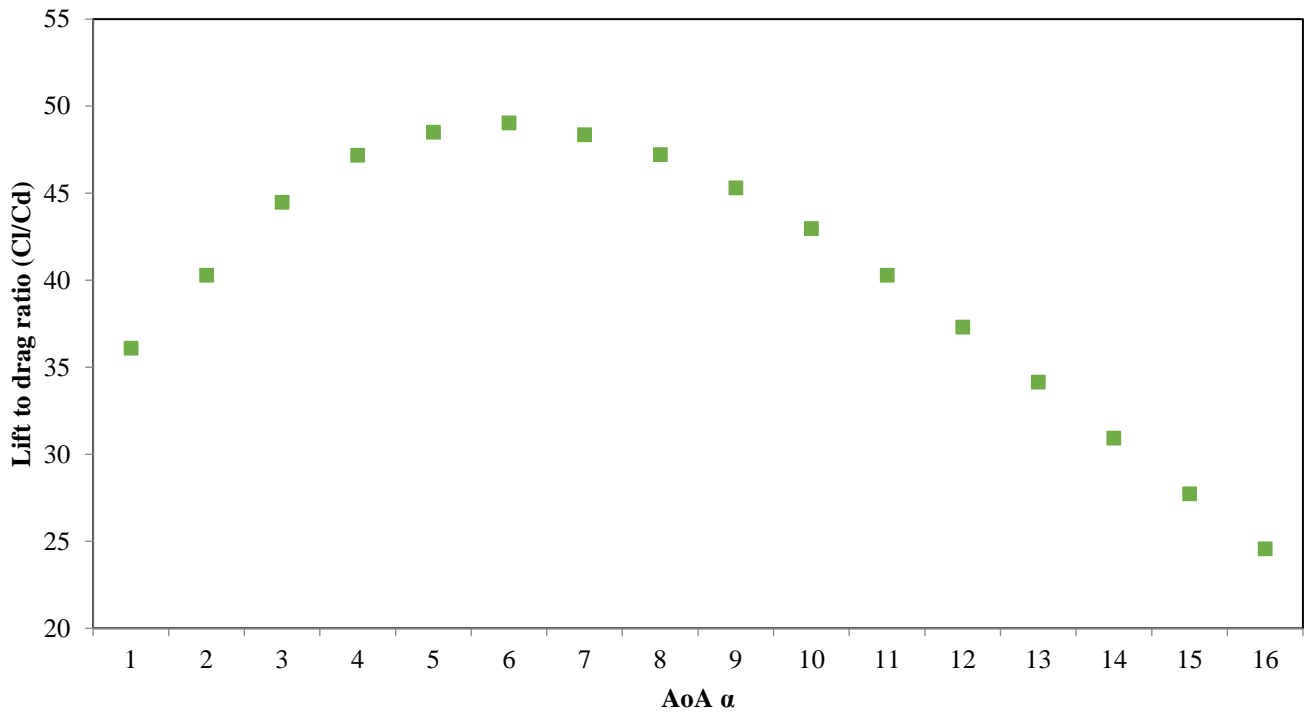
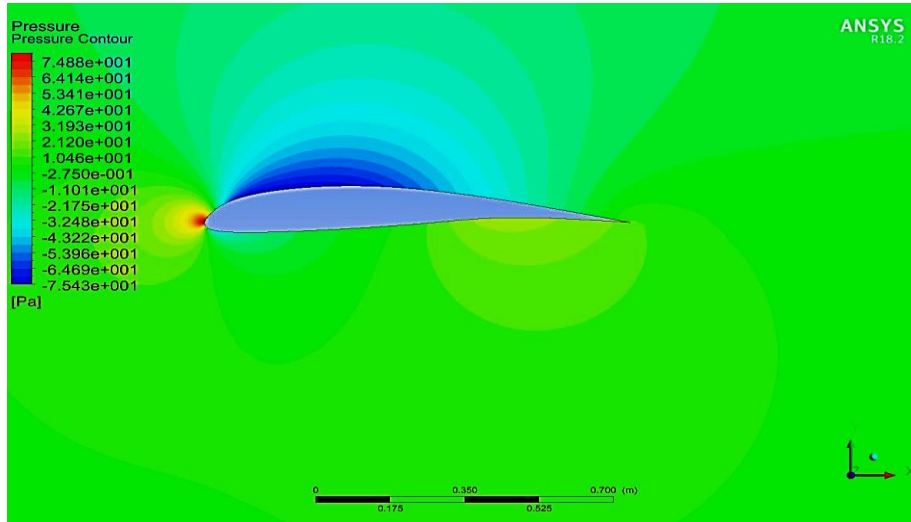
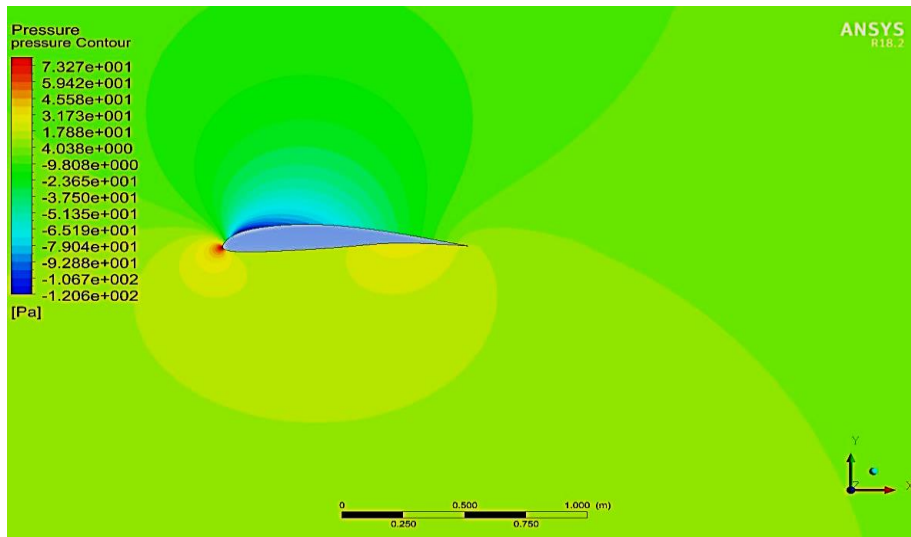


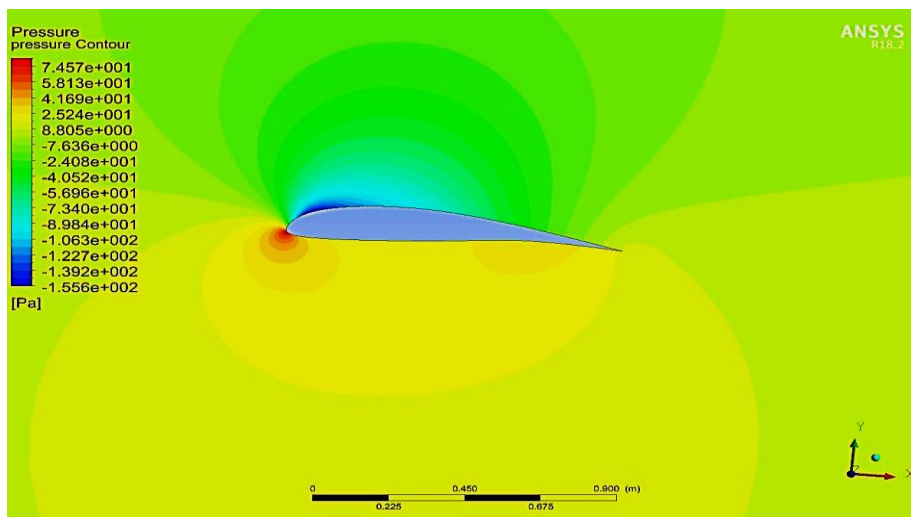
Fig. 11  $C_l/C_d$  ratio of airfoil during 2D CFD simulation



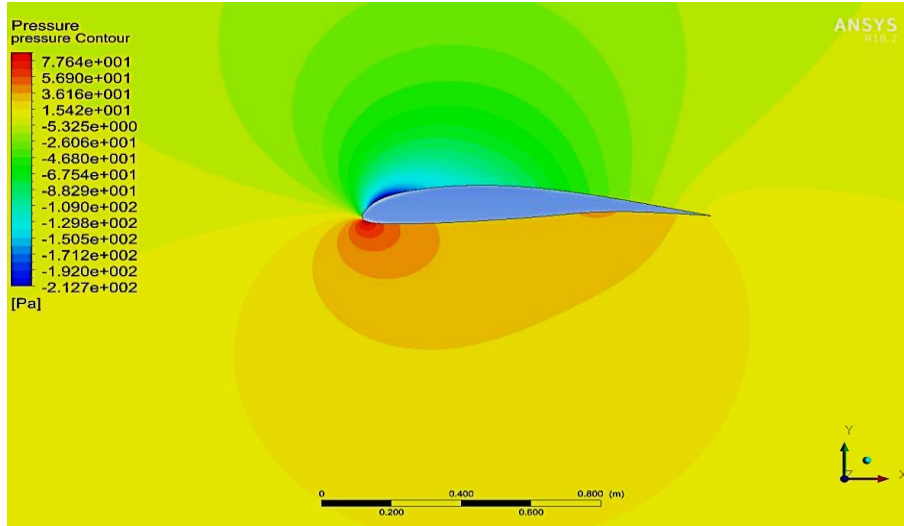
(a) AoA 0°



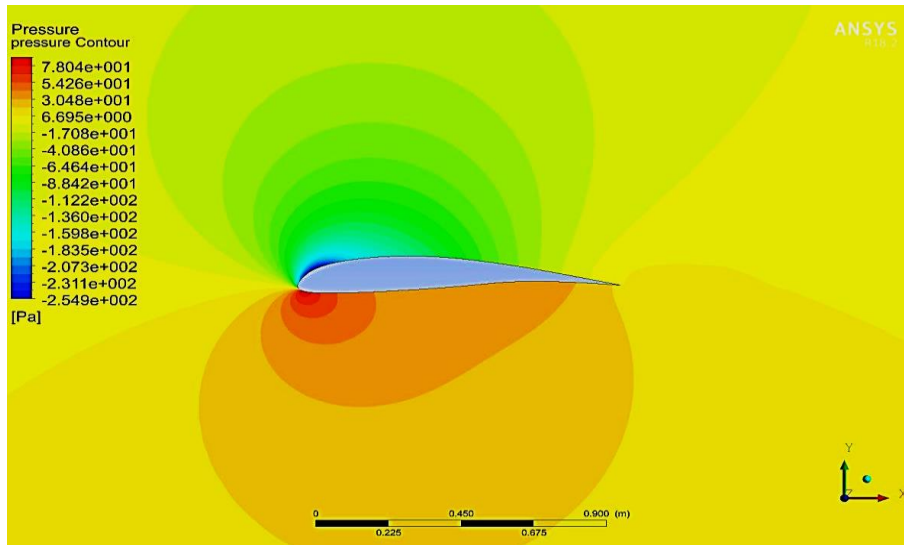
(b) AoA 3°



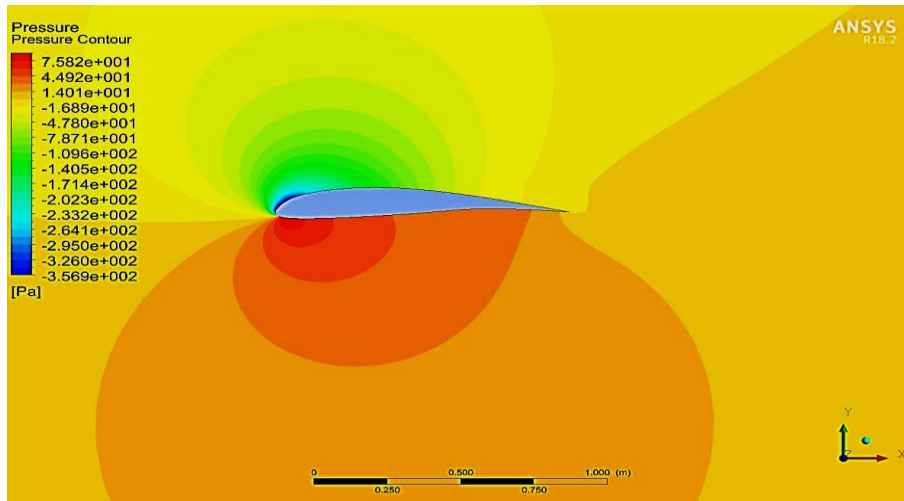
(c) AoA 5°



(d) AoA 8°

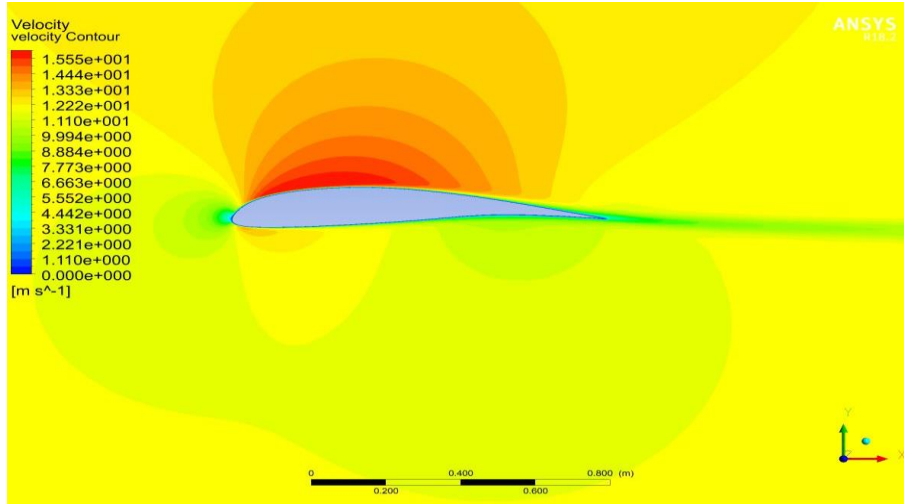


(e) AoA 10°

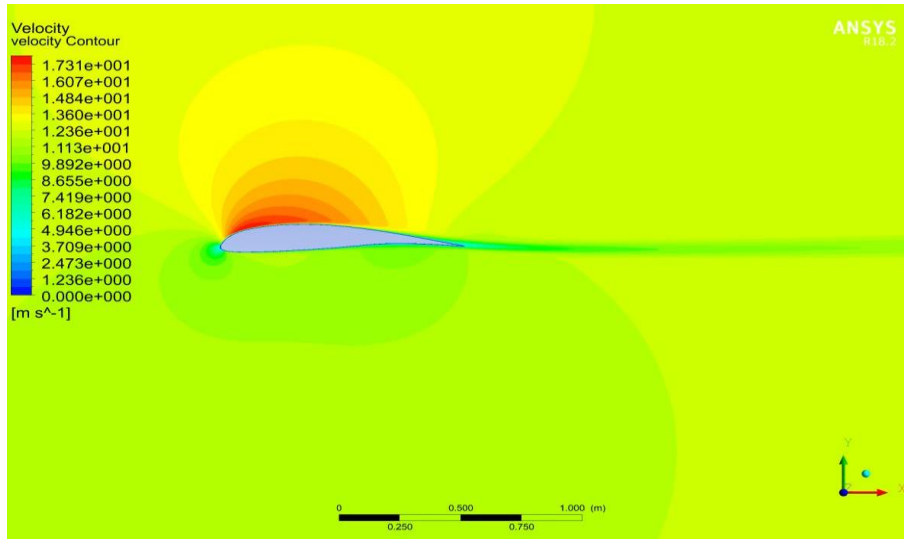


(f) AoA 15°

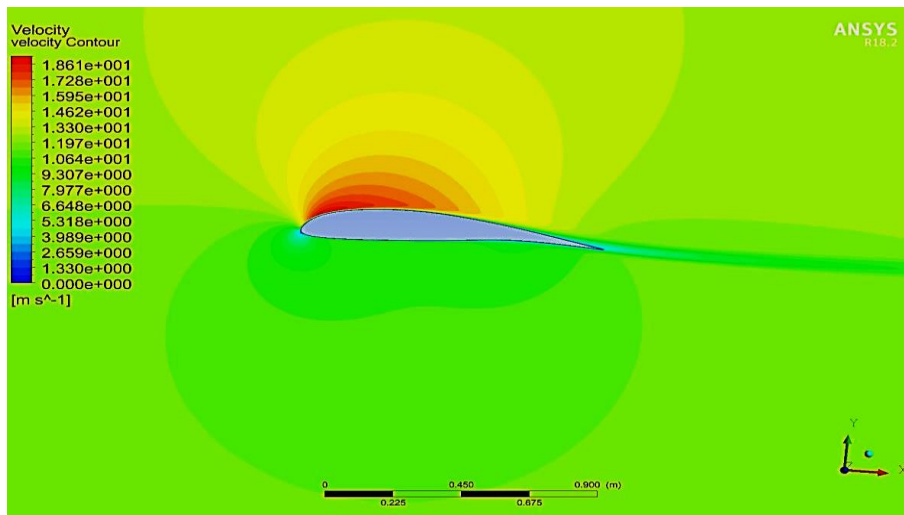
Fig. 12 Contours of pressure at various  $\alpha$  angles for an airfoil



(a) AoA 0°



(b) AoA 3°



(c) AoA 5°

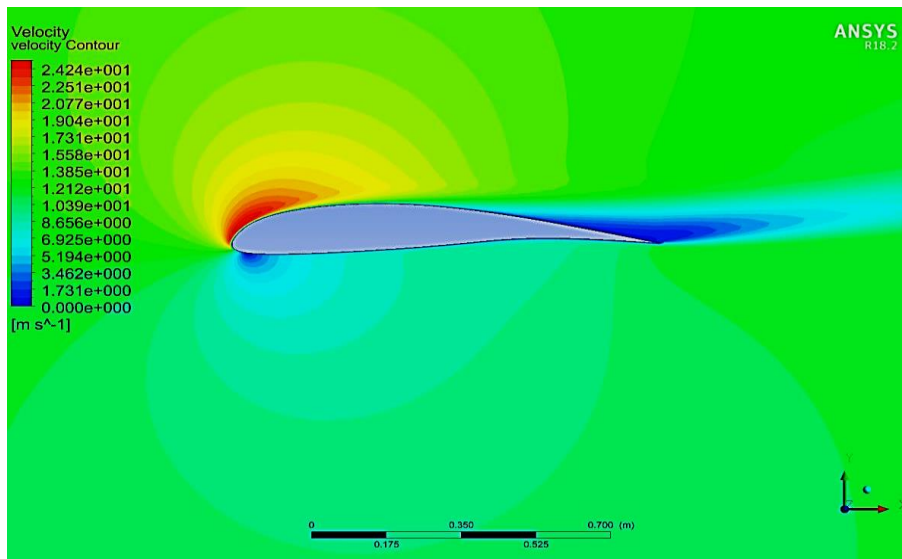
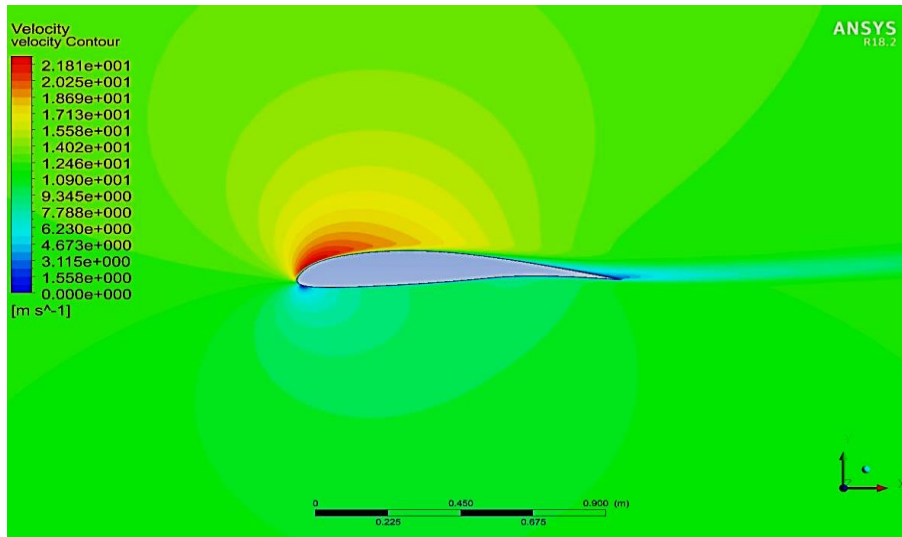
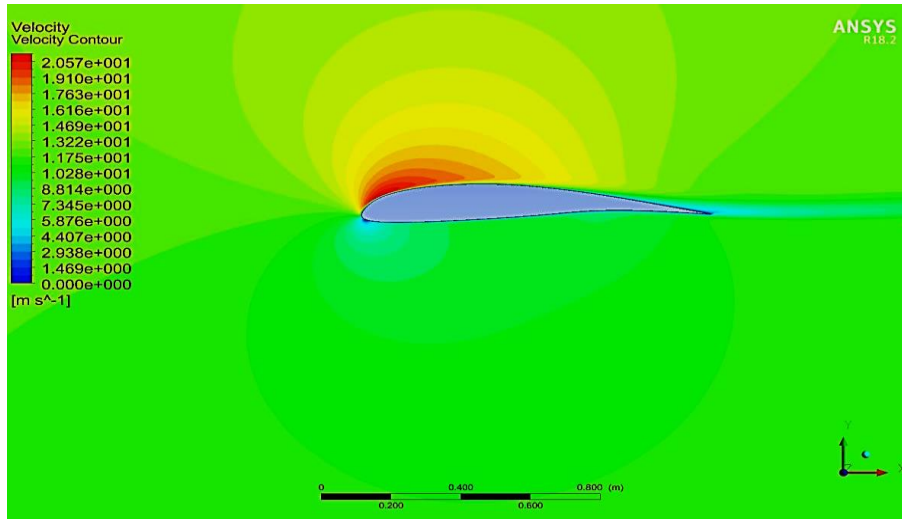


Fig. 13 Velocity contours at various  $\alpha$  angles for an airfoil

### 4. 3D CFD Simulation of an Airfoil

The two identical curves placed at a 0.8 m distance apart in the z-axis were prepared using solid works. These curves were converted into the surface, and then they were joined using a skin tool.

Fig. 14 shows the domain names given as airfoil, inlet and outlet. Fig. 15 shows the automatic meshing was performed by selecting the six airfoil edges. The number of divisions on each edge was given as 50.

The standard wall function of turbulent model k-ε was selected. It takes advantage of both models, namely kinetic energy and energy dissipation rate. During large pressure gradients at boundary layers, this model gives good results. The air was selected as fluid material with wind speed, air density, kinematic viscosity, enthalpy and the ratio of specific heat as 12m/s, 1.22 kg/m<sup>3</sup>, 1.7894 × 10<sup>-5</sup> kg/m-s, 23546.47, 1.4 respectively.

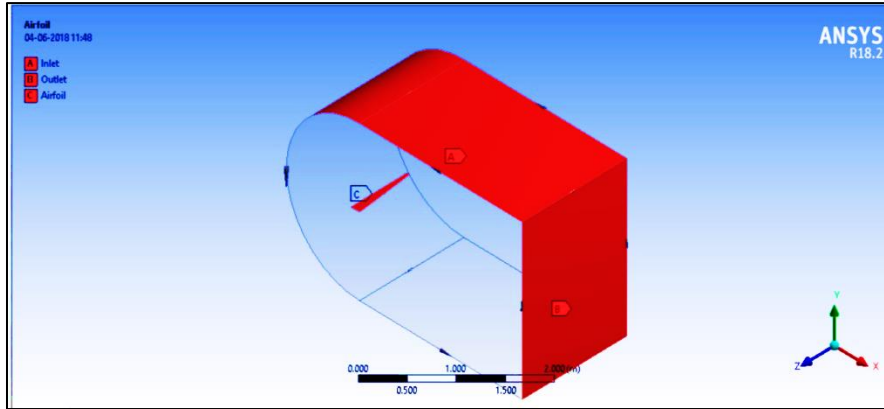


Fig. 14 Name selection

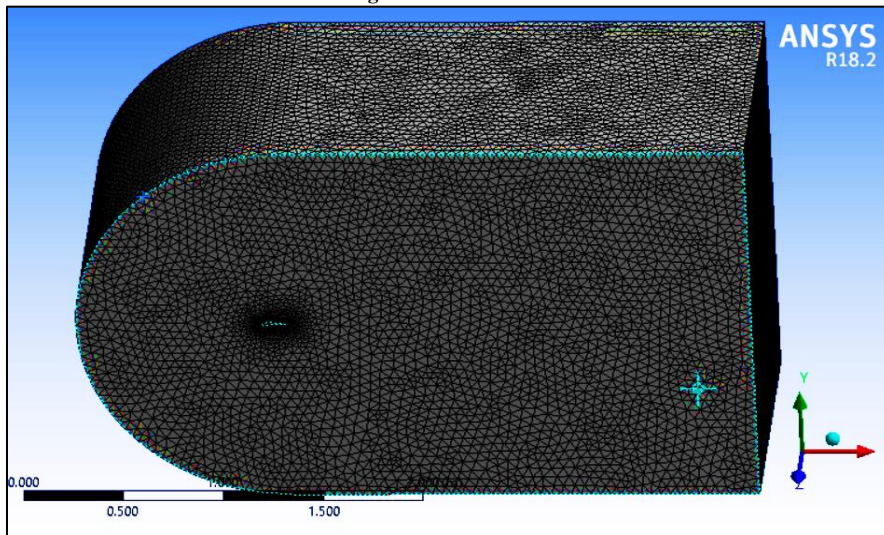


Fig. 15 Meshing of the blade enclosure

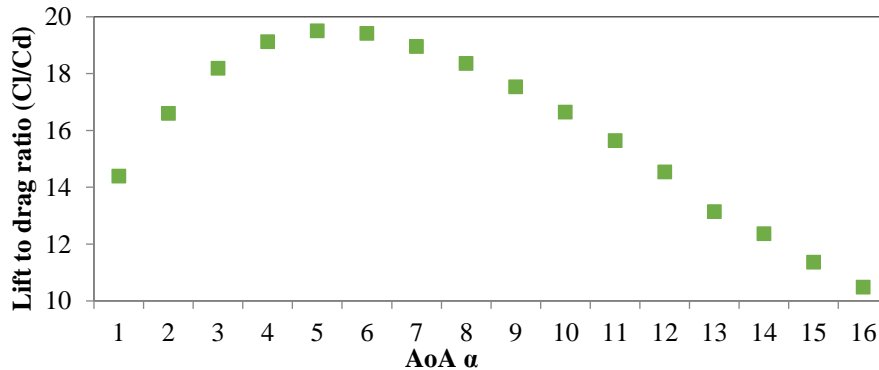


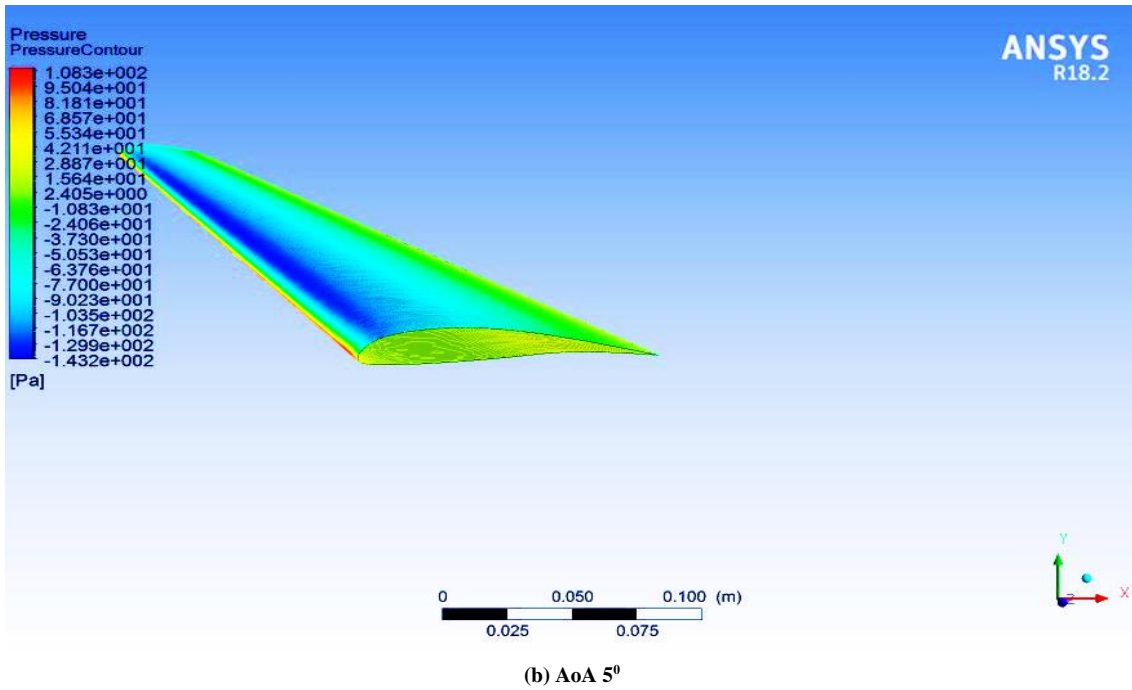
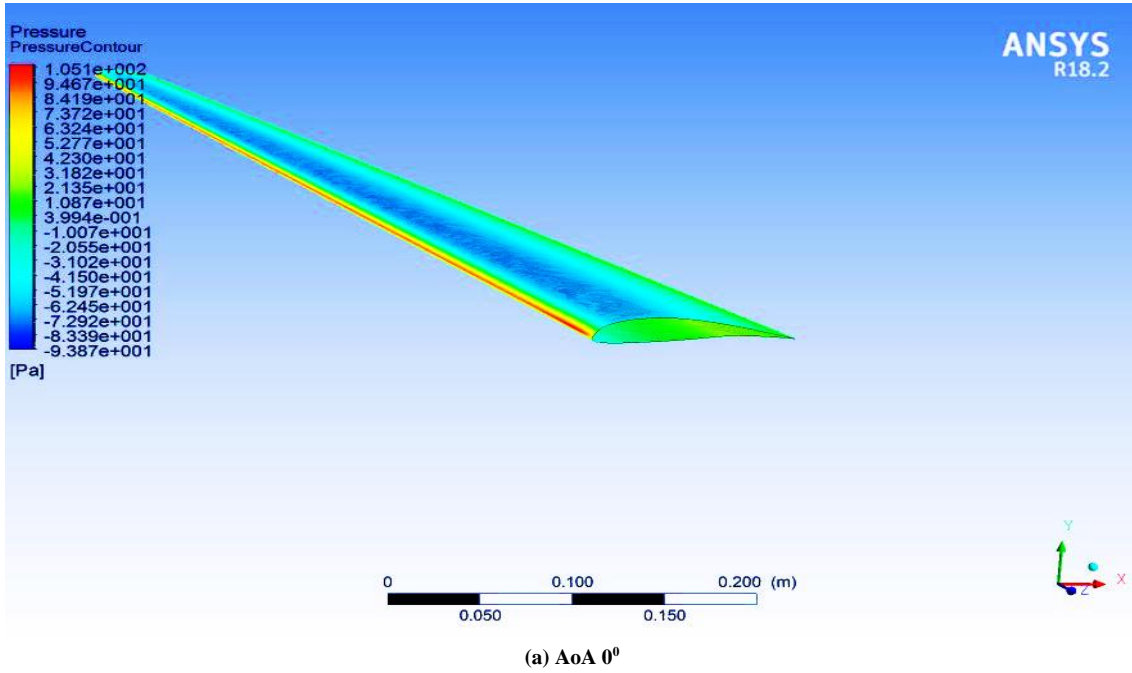
Fig. 16 Coefficient of the lift-to-drag ratio of a blade

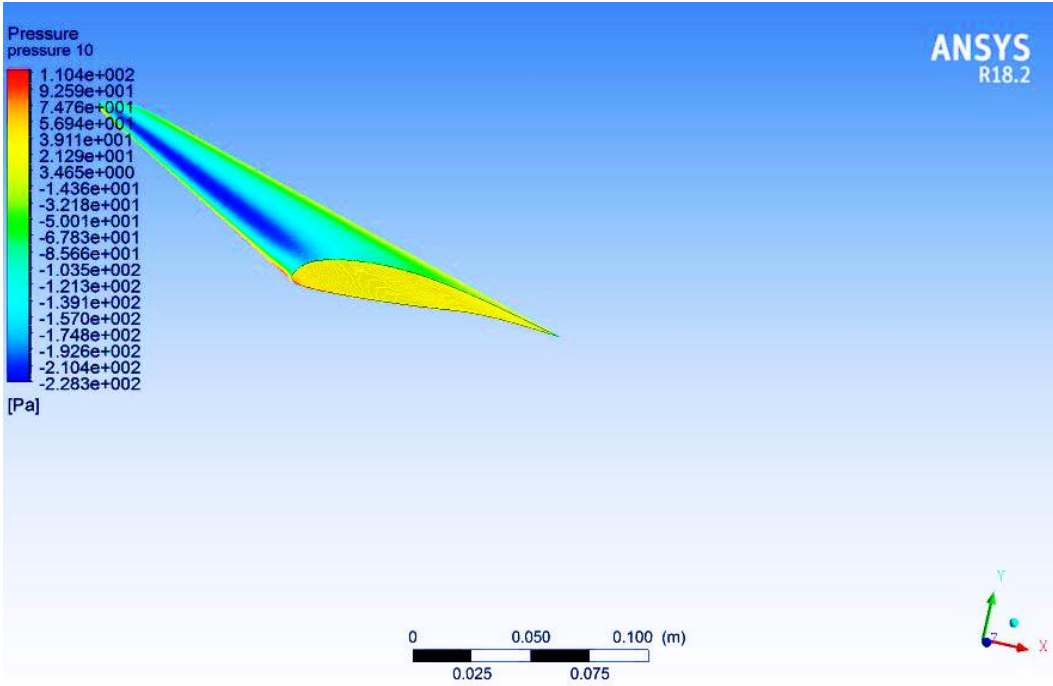
**4.1. 3D CFD (FLUENT) Analysis Result**

The blade was analyzed for lift and drag coefficient parameters. Fig. 16 indicates that  $C_l/C_d$  ratio reaches its optimum value at  $\alpha = 4^\circ$ , and after that, it decreases. The lift, drag coefficient and maximum value of the  $C_l/C_d$  ratio were obtained as 0.0519, 0.00266 and 19.51 at an angle ( $\alpha$ )  $4^\circ$ .

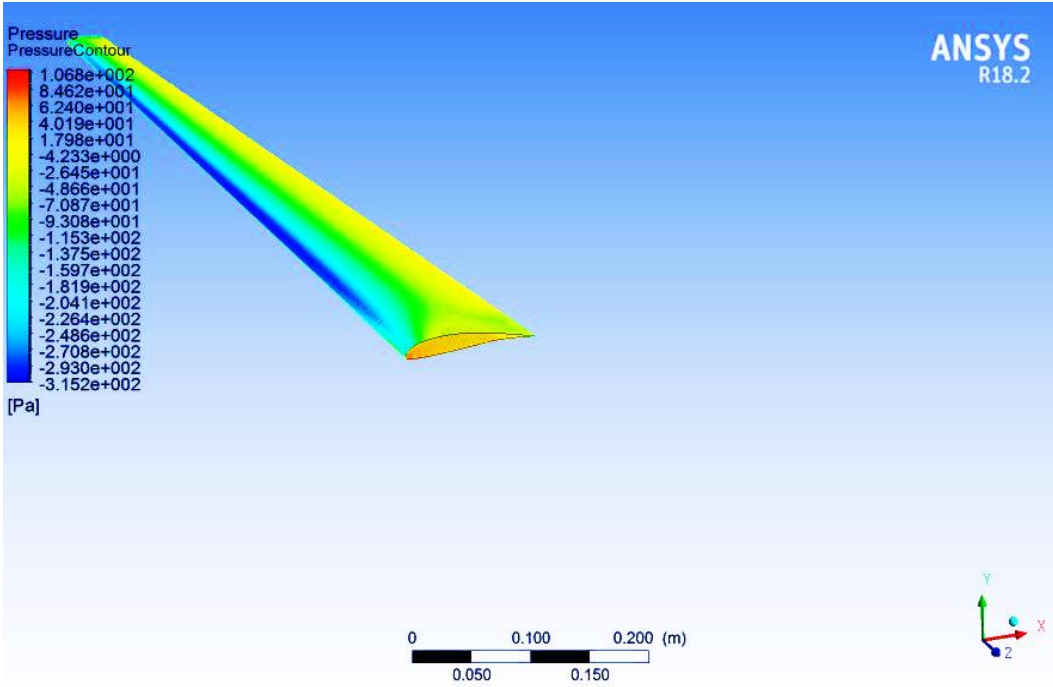
The top surface of the blade was subjected to low pressure, while the lower edge of the blade and the leading edge were subjected to high pressure. The high pressure on the lower side of the blade causes the blade to lift in an upward direction due to lifting force. The blade's position is normal to the airflow stream. The maximal value of the  $C_l/C_d$  ratio was obtained for the value of  $\alpha$  in the range of  $4^\circ$  to  $6^\circ$ . The main reason behind this was that, during these angles, pressures at the lower blade surface were more and upper surface drag was less.

Fig. 17 (a-d) shows pressure contours at various angles  $\alpha$ . The simulation was performed using a density-based solver.





(c) AoA 10°

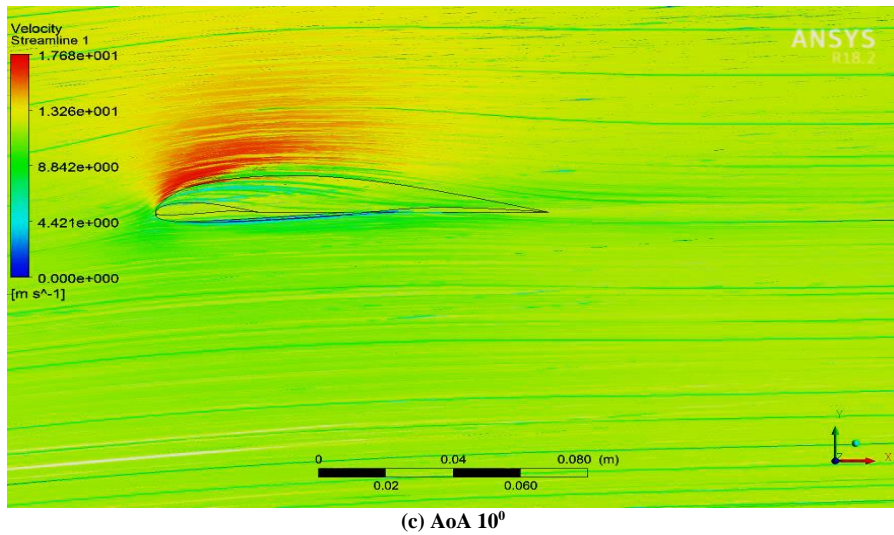
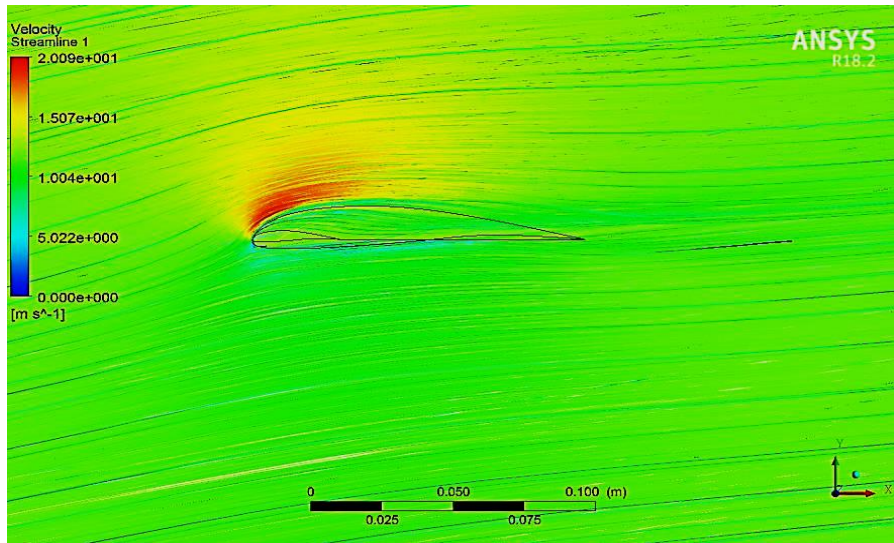
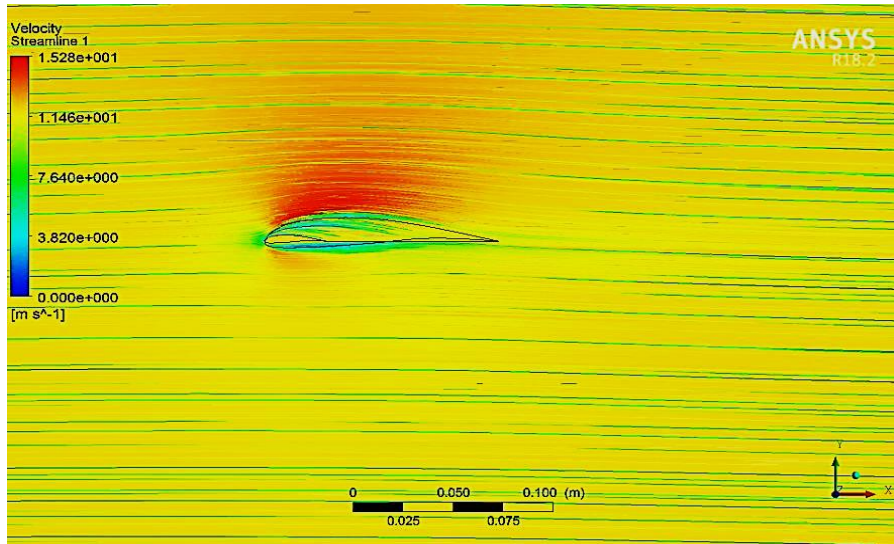


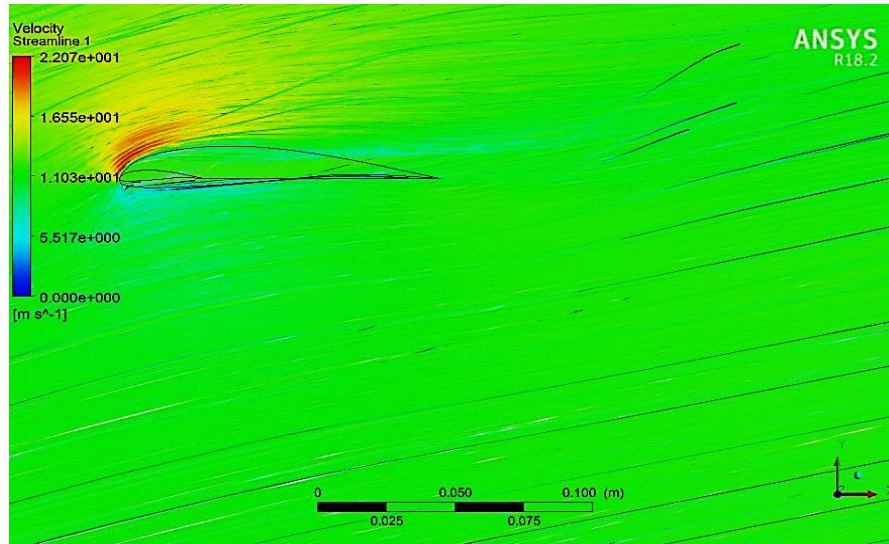
(d) AoA 15°

Fig. 17 Pressure contours at various  $\alpha$  angles for the blade

Fig. 18 (a-d) shows CFD simulation at various  $\alpha$  angles of velocity streamline. These simulations were obtained for a density-based solver. The boundary layer separation has initiated on the leading edge, and the velocity of the stream is roughly zero. The maximum and minimum flow velocities were obtained at the blade's top surface and lower portion,

respectively. As the AoA reaches 10° or above, the backflow is generated (vertex) at the trailing edge. The backflow increases  $C_d$  and reduces the efficiency of the blade. The Value of AoA should be selected so that the maximum value of the  $C_l / C_d$  ratio might be obtained.





(d) AoA 15°  
 Fig. 18 Velocity Streamline at various  $\alpha$  angles for the blade

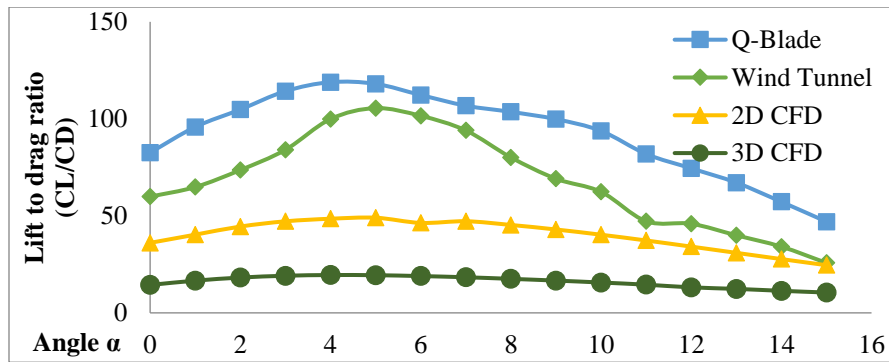


Fig. 19 Coefficient lift-to-drag ratio of Q-Blade, Wind tunnel, 2D and 3D simulation

## 5. Result and Discussion

Fig. 19 represents lift to drag ratio for Q-Blade, CFD simulation and wind tunnel experimental result for values of  $\alpha$  in the range of  $0^{\circ}$ - $15^{\circ}$ . The wind tunnel results show a maximum  $C_l/C_d$  ratio of 105.50 was obtained at  $\alpha = 5^{\circ}$  with  $C_l$  and  $C_d$  as 0.939 and 0.0090, respectively. The results obtained through experimentation on wind tunnel, Q Blade and CFD simulation show a maximum value of  $C_l/C_d$  ratio at  $\alpha = 5^{\circ}$ . The 2D and 3D simulation results represent the highest  $C_l/C_d$  ratio at  $\alpha = 5^{\circ}$ . Koç et al. [29] analyzed comparing Q-Blade and CFD simulation results for small-scale wind turbines at transient conditions. Analyzed the comparison between the Blade Element Method and CFD simulations of wind turbines [30,31]. The values corresponding to lift and drag co-efficient differ in 2D and 3D simulation. During 2D simulation, only the surface of the airfoil was selected, while during 3D simulation, the entire blade geometry, along with the twist angle, was considered.

## 6. Conclusion

The micro-scale wind turbine performance is mostly affected due to environmental constraints viz; wind speed,

temperature and location. Airfoil with aerodynamic profile plays a crucial role while designing high-performance wind turbines. Pressure and velocity distribution profiles were obtained by performing Q-Blade and CFD simulations.

The Q-Blade approach reveals that at  $\alpha = 5^{\circ}$ ,  $C_l$ ,  $C_d$ , and  $C_l/C_d$  ratios were 1.028, 0.0085 and 120.94, respectively. When  $\lambda$  is 7,  $C_p$  has a high value of 0.45. Airfoil 2D CFD analysis using the standard k- $\epsilon$  turbulent model shows that  $C_l/C_d$  ratio has a maximum value of 49.04 at  $\alpha = 5^{\circ}$  and decreases due to increased drag force. The corresponding value of  $C_l$  and  $C_d$  were 1.09 and 0.022, respectively.

A blade CFD result reveals that  $C_l/C_d$  ratio obtains its maximum value at  $\alpha = 4^{\circ}$  and later it decreases. The  $C_l$ ,  $C_d$  coefficient and maximum value of the  $C_l/C_d$  ratio were obtained as 0.0519, 0.00266 and 19.51 at an angle ( $\alpha$ )  $4^{\circ}$ . The wind tunnel approach reveals a maximum  $C_l/C_d$  ratio of 105.50 was obtained at  $\alpha = 5^{\circ}$  with  $C_l$  and  $C_d$  as 0.939 and 0.0090, respectively. Hence, the maximum  $C_l/C_d$  ratio can be obtained by keeping the AoA in the scope of  $4^{\circ}$  to  $5^{\circ}$ .

## References

- [1] Ministry of Statistics and Programme Implementation, National Statistical Office, Government of India, Energy Statics India, 2023. [Online]. Available: <https://www.mospi.gov.in/>
- [2] K. R. Rao, "Wind Energy for Power Generation: Meeting the Challenge of Practical Implementation," *Springer International Publishing*, 2019. [[CrossRef](#)] [[Google Scholar](#)] [[Publisher Link](#)]
- [3] David W. Keith et al., "The Influence of Large-Scale Wind Power on Global Climate," *Proceedings of the National Academy of Sciences*, vol. 101, no. 46, pp. 16115-16120, 2004. [[CrossRef](#)] [[Google Scholar](#)] [[Publisher Link](#)]
- [4] B H Fiedler, and M S Bukovsky, "The Effect of a Giant Wind Farm on Precipitation in a Regional Climate Model," *Environmental Research Letters*, vol. 6, no. 4, 2011. [[CrossRef](#)] [[Google Scholar](#)] [[Publisher Link](#)]
- [5] Abhishiktha Tummala et al., "A Review on Small Scale Wind Turbines," *Renewable and Sustainable Energy Reviews*, vol. 56, pp. 1351-1371, 2016. [[CrossRef](#)] [[Google Scholar](#)] [[Publisher Link](#)]
- [6] Jakub Bukala et al., "Investigation of Parameters Influencing the Efficiency of Small Wind Turbines," *Journal of Wind Engineering and Industrial Aerodynamics*, vol. 146, pp. 29-38, 2015. [[CrossRef](#)] [[Google Scholar](#)] [[Publisher Link](#)]
- [7] Abdoukader Ibrahim Idrisset al., "Wind Energy Potential and Micro-Turbine Performance Analysis in Djibouti-City, Djibouti," *Engineering Science and Technology, An International Journal*, vol. 23, no. 1, pp. 65-70, 2020. [[CrossRef](#)] [[Google Scholar](#)] [[Publisher Link](#)]
- [8] Arvind Prabhakar, "CFD Analysis of Static Pressure and Dynamic Pressure for NACA 4412," *International Journal of Engineering Trends and Technology*, vol. 4, no. 8, pp. 3258-3265, 2013. [[Google Scholar](#)] [[Publisher Link](#)]
- [9] Kazumasa Ameku, Baku M. Nagai, and Jitendro Nath Roy, "Design of a 3 kW Wind Turbine Generator with Thin Airfoil Blades," *Experimental Thermal and Fluid Science*, vol. 32, no. 8, pp. 1723-1730, 2008. [[CrossRef](#)] [[Google Scholar](#)] [[Publisher Link](#)]
- [10] Abolfazl Pourrajabian, Reza Ebrahimi, and Masoud Mirzaei, "Applying Micro Scales of Horizontal Axis Wind Turbines for Operation in Low Wind Speed Regions," *Energy Conversion and Management*, vol. 87, pp. 119-127, 2014. [[CrossRef](#)] [[Google Scholar](#)] [[Publisher Link](#)]
- [11] Onder Ozgener, "A Small Wind Turbine System Application and its Performance Analysis," *Energy Conversion and Management*, vol. 47, no. 11-12, pp. 1326-1337, 2006. [[CrossRef](#)] [[Google Scholar](#)] [[Publisher Link](#)]
- [12] Ankan Dash, "CFD Analysis of Wind Turbine Airfoil at Various Angles of Attack," *IOSR Journal of Mechanical and Civil Engineering*, vol. 13, pp. 18-24, 2016. [[CrossRef](#)] [[Google Scholar](#)] [[Publisher Link](#)]
- [13] Ji Yao et al., "Numerical Simulation of Aerodynamic Performance for Two Dimensional Wind Turbine Airfoils," *Procedia Engineering*, vol. 31, pp. 80-86, 2012. [[CrossRef](#)] [[Google Scholar](#)] [[Publisher Link](#)]
- [14] Rodrigo M. Rodrigues et al., "Development of Guidelines for the Construction of Wind Turbines using Scrap Material," *Procedia Engineering*, vol. 159, pp. 292-299, 2016. [[CrossRef](#)] [[Google Scholar](#)] [[Publisher Link](#)]
- [15] Jasminder Singh et al., "Study of NACA 4412 and Selig 1223 Airfoils through Computational Fluid Dynamics," *SSRG International Journal of Mechanical Engineering*, vol. 2, no. 6, pp. 17-21, 2015. [[CrossRef](#)] [[Google Scholar](#)] [[Publisher Link](#)]
- [16] João P. Monteiro et al., "Wind Tunnel Testing of a Horizontal Axis Wind Turbine Rotor and Comparison with Simulations from Two Blade Element Momentum Codes," *Journal of Wind Engineering and Industrial Aerodynamics*, vol. 123, pp. 99-106, 2013. [[CrossRef](#)] [[Google Scholar](#)] [[Publisher Link](#)]
- [17] Manwell, James, Jon G. MCGowan, and A. L. Rogers, "Wind Energy Explained: Theory, Design and Application," *John Wiley & Sons*, 2010. [[Google Scholar](#)]
- [18] Abhishek Choubey, Prashant Baredar, and Neha Choubey, "Power Optimization of National Advisory Committee for Aeronautics 0018 Airfoil Blade of Horizontal Axis Wind Turbine by Computational Fluid Dynamics Analysis," *International Journal of Energy Optimization and Engineering*, vol. 9, no. 1, pp. 122-139, 2020. [[CrossRef](#)] [[Google Scholar](#)] [[Publisher Link](#)]
- [19] Vincent Anayochukwu Ani, "Optimal Energy System for Single Household in Nigeria," *International Journal of Energy Optimization and Engineering*, vol. 2, no. 3, pp. 16-41, 2013. [[CrossRef](#)] [[Google Scholar](#)] [[Publisher Link](#)]
- [20] Siegfried Heier, "Grid Integration of Wind Energy Conversion Systems," John Wiley & Sons, New York, 1998.
- [21] Nadia Bizzarrini, Francesco Grasso, and Domenico Coiro, "Genetic Algorithms in Wind Turbine Airfoil Design," *EWEA, EWEC2011, Bruxelles, Belgium*, pp. 14-17, 2011. [[Google Scholar](#)] [[Publisher Link](#)]
- [22] Ernesto Benini, and Andrea Toffolo, "Optimal Design of Horizontal-Axis Wind Turbines using Blade-Element Theory and Evolutionary Computation," *Journal of Solar Energy Engineering*, vol. 124, no. 4, pp. 357-363, 2002. [[CrossRef](#)] [[Google Scholar](#)] [[Publisher Link](#)]
- [23] Liu, Xiongwei, Lin Wang, and Xinzi Tang, "Optimized Linearization of Chord and Twist Angle Profiles for Fixed-Pitch Fixed-Speed Wind Turbine Blades," *Renewable Energy*, vol. 57, pp. 111-119, 2013. [[CrossRef](#)] [[Google Scholar](#)] [[Publisher Link](#)]
- [24] Nishant Kumar, Saurav Upadhaya, and Ashish Rohilla, "Evaluation of the Turbulence Models for the Simulation of the Flow Over a Tsentralniy Aerogidrodinamicheskoy Institut -12% Airfoil," *SSRG International Journal of Mechanical Engineering*, vol. 4, no. 1, pp. 18-28, 2017. [[CrossRef](#)] [[Google Scholar](#)] [[Publisher Link](#)]

- [25] Douvi C. Eleni, Tsavalos I. Athanasios, and Margaris P. Dionissios, "Evaluation of the Turbulence Models for the Simulation of the Flow Over a National Advisory Committee for Aeronautics 0012 Airfoil," *Journal of Mechanical Engineering Research*, vol. 4, no. 3, pp. 100-111, 2012. [[CrossRef](#)] [[Google Scholar](#)] [[Publisher Link](#)]
- [26] Ronit K. Singh, and M. Rafiuddin Ahmed, "Blade Design and Performance Testing of a Small Wind Turbine Rotor for Low Wind Speed Applications," *Renewable Energy*, vol. 50, pp. 812-819, 2013. [[CrossRef](#)] [[Google Scholar](#)] [[Publisher Link](#)]
- [27] Minendra L. Surve et al., "Computational Studies on Airfoil for Micro-Capacity Horizontal Axis Wind Turbine," *Indian Journal of Science and Technology*, vol. 14, no. 29, pp. 2427-2438, 2021. [[CrossRef](#)] [[Google Scholar](#)] [[Publisher Link](#)]
- [28] Mayurkumar Kevadiya, and Hemish Vaidya, "2d Analysis of National Advisory Committee for Aeronautics 4412 Airfoil," *International Journal of Innovative Research in Science, Engineering and Technology*, vol. 2, no. 5, 2013. [[Google Scholar](#)] [[Publisher Link](#)]
- [29] Emre Koç, Onur Günel, and Tahir Yavuz, "Comparison of QBLADE and Computational Fluid Dynamics Results for Small-Scaled Horizontal Axis Wind Turbine Analysis," *IEEE International Conference on Renewable Energy Research and Applications*, pp. 204-209, 2016. [[CrossRef](#)] [[Google Scholar](#)] [[Publisher Link](#)]
- [30] Galih Bangga, "Comparison of Blade Element Method and Computational Fluid Dynamics Simulations of a 10 MW Wind Turbine," *Fluids*, vol. 3, no. 4, p. 73, 2018. [[CrossRef](#)] [[Google Scholar](#)] [[Publisher Link](#)]
- [31] Borja Plaza, Rafael Bardera, and Sergio Visiedo, "Comparison of Blade Element Momentum and Computational Fluid Dynamics Results for Mexico Rotor Aerodynamics," *Journal of Wind Engineering and Industrial Aerodynamics*, vol. 145, pp. 115-122, 2015. [[CrossRef](#)] [[Google Scholar](#)] [[Publisher Link](#)]
- [32] Meng-Hsien Lee, Y.C. Shiah, and Chi-Jeng Bai, "Experiments and Numerical Simulations of the Rotor-Blade Performance for a Small-Scale Horizontal Axis Wind Turbine," *Journal of Wind Engineering and Industrial Aerodynamics*, vol. 149, pp. 17-29, 2016. [[CrossRef](#)] [[Google Scholar](#)] [[Publisher Link](#)]
- [33] Abdulkadir Ali et al., "An Aerodynamic Study of a Domestic Scale Horizontal Axis Wind Turbine with Varied Tip Configurations," *Procedia Engineering*, vol. 105, pp. 757-762, 2015. [[CrossRef](#)] [[Google Scholar](#)] [[Publisher Link](#)]
- [34] David Marten et al., "QBLADE: An Open Source Tool for Design and Simulation of Horizontal and Vertical Axis Wind Turbines," *International Journal of Emerging Technology and Advanced Engineering*, vol. 3, no. 3, pp. 264-269, 2013. [[Google Scholar](#)] [[Publisher Link](#)]